Nonlinear Dyn
https://doi.org/10.1007/s11071-024-10605-y

RESEARCH

Riemann-hilbert problem and physics-informed neural networks method for the nonlocal Sasa-Satsuma equation

Wen-Xin Zhang · **Yong Chen**

Received: 23 July 2024 / Accepted: 4 November 2024

Abstract This paper investigates N-soliton and data-driven solutions of a novel nonlocal Sasa-Satsuma (SS) equation by applying the Riemann-Hilbert problem and the physics-informed neural networks (PINN) method. Based on the zero curvature formulation with arbitrary order spatial and temporal spectral matrixes, the novel nonlocal SS equation is constructed from the nonlocal integrable SS hierarchies possessing the bi-Hamiltonian structures and the Liouville integrability. Analyzing properties of the Jost matrix, the Riemann-Hilbert problem and some novel symmetry constraints are derived for obtaining the N-soliton solutions of the nonlocal SS equation. Moreover, the dynamic characteristics of these one- and two-soliton solutions are visually displayed in some figures. Finally, the data-driven solutions of the nonlocal SS equation are availably learned via the PINN approach combining with the spatial and temporal nonlocal terms. And the results show the error range between the predicted data-driven solutions and the exact solutions, which indicate the effectiveness of the method.

W.-X. Zhang · Y. Chen
School of Mathematical Sciences, Key Laboratory of PMMP, Key Laboratory of Mathematics and Engineering Applications (Ministry of Education) and Shanghai, East China Normal University, 200241 Shanghai, China

Y. Chen (✉)
College of Mathematics and Systems Science, Shandong University of Science and Technology, 266590 Qingdao, China
e-mail: ychen@sei.ecnu.edu.cn

Keywords Nonlocal Sasa-Satsuma equation · Nonlocal integrable Sasa-Satsuma hierarchies · Riemann-hilbert problem · Physics-informed neural networks method

1 Introduction

As well as we know, many nonlinear partial differential equations (PDEs) have quite rich physical significance. As a kind of important nonlinear PDE, nonlinear Schrödinger (NLS) equation [1] was extensively investigated in the realm of mathematical physics, such as hydrodynamics [2], nonlinear optical fibers [3], Bose-Einstein condensates [4] and ion acoustic waves [5] with nonlinear instability. The Sasa-Satsuma (SS) equation is one of the higher-order NLS equations, which can be applied to monomode optical fibers [6]. It is worth mentioning that the SS equation has diversiform dynamic features of solutions, such as semirational rogue-wave solutions [7], general breather solutions [8], single- and double-hump solitons [9,10], and so on. Additionally, the Riemann-Hilbert problem [11,12] is an effective method to obtain various dynamic behaviors of solutions for the SS equation. According to a spectral analysis of its Lax pair, Geng and Wu established the corresponding Riemann-Hilbert method of the generalized SS equation [13]. Based on a standard dressing procedure of the SS equation, Yang and Chen constructed simple and high-order zeros in the Riemann-Hilbert problem [14]. On account

Published online: 12 November 2024

of a multi-component SS hierarchies, Liu et al. studied the generalized coupled Sasa-Satsuma equation by the Riemann-Hilbert method and analyzed the asymptotic behaviors of two-soliton solutions [15].

Since Ablowitz and Musslimani [16] investigated the nonlocal NLS equation through the inverse scattering transform, some related research on nonlocal equations had gradually entered the view of scholars. It can be noted that numerous approaches (Darboux transformations [17,18], Riemann-Hilbert approach [19,20], for instance) applied to local equations as well as nonlocal equations. As one kind of nonlocal equation, the nonlocal SS equation was studied to get novel dynamic behaviors of soliton solutions via the binary Darboux transformation method [21] and inverse scattering transformation [22–24]. Moreover, the infinite conservation law and the bi-Hamiltonian structure of a nonlocal SS equation were deduced, and the relationship between a nonlocal SS equation and a Heisenberg-like equation was constructed [25]. In this paper, a novel nonlocal SS equation with the space-time nonlocal term is obtained by the nonlocal integrable SS hierarchies rigorously derived in Sect. 2. This novel nonlocal SS equation has some novel symmetric constraints of discrete scattering data and scattering matrix, which is considered as the following form

$$\begin{aligned} &q_t + q_{xxx} + 6(q(-x,-t)q^* + qq^*(-x,-t))q_x \\ &+3q(qq^*(-x,-t) + q^*q(-x,-t))_x = 0, \end{aligned} \tag{1}$$

where $q = q(x,t)$ represents a complex-valued potential function, and $q^* = q^*(x,t)$ shows as the complex conjugate function of q. The nonlocality of equation (1) manifests itself in the fact that the solutions make sense at two different space and time locations (x,t) and $(-x,-t)$ simultaneously [26]. This means that the novel nonlocal SS equation has the new spatial and temporal coupling different from the local SS equation, which can give some novel symmetry analysis for discrete scattering data as well as exquisite and additional solution characteristics. To indicate the integrability of the nonlocal SS equation (1), its Lax pair is presented as follows

$$-iY_x = UY, \quad -iY_t = VY, \tag{2}$$

where $Y = Y(x,t,z)$ is a eigenfunction with a complex spectral parameter z, and

$$U = z\Lambda + Q, \quad V = 4z^3\Lambda + P, \tag{3}$$

where

$$\Lambda = \mathrm{diag}(1,1,1,1,-1), \tag{4}$$

$$Q = \begin{pmatrix} 0 & 0 & 0 & 0 & -iq \\ 0 & 0 & 0 & 0 & -iq^* \\ 0 & 0 & 0 & 0 & -iq(-x,-t) \\ 0 & 0 & 0 & 0 & -iq^*(-x,-t) \\ iq^*(-x,-t) & iq(-x,-t) & iq^* & iq & 0 \end{pmatrix}, \tag{5}$$

and

$$\begin{aligned} P = &4z^2Q - 2iz(iQ^2 + Q_x)\Lambda + iQ_xQ - iQQ_x \\ &-Q_{xx} - 2Q^3. \end{aligned} \tag{6}$$

Based on the spatial and temporal parts of the above Lax pair (2), the nonlocal SS equation (1) can be derived by the zero curvature formula $U_t - V_x + i[U, V] = 0$.

In addition, with the development of computational speed and accuracy, deep neural network algorithms were extended to the field of calculations for forward and inverse problems of PDEs [27–29]. Combining with the physical laws satisfied by nonlinear PDEs, Raissi et al. proposed a physics-informed neural networks (PINN) algorithm, which provided a new inspiration for people to explore data-driven solutions and data-driven discovery of nonlinear PDEs [27]. Based on the PINN method, plentiful dynamic features of solutions of abundant equations can be reproduced successfully, such as data-driven breather solutions [30,31] and the rogue wave solutions [32–34]. Furthermore, on account of the main ideas of PINNs, a lot of improved neural network frameworks were put forward, including the two-stage PINN [35], the Lax pairs informed neural networks (LPNNs) [36], the initial-value iterative neural network (IINN) [37], etc. Similarly, the PINN method can also be used to predict various dynamic behaviors of solutions in nonlocal systems [38–40]. Zhang et al. investigated the nonlocal Davey-Stewartson (DS) I equation with an improved PINN method, in which the PT symmetric constraint and the model were led into the loss function [41]. Peng and Chen studied the forward and inverse problems of the nonlocal NLS equation, the nonlocal derivative NLS equation and the nonlocal three-wave interaction systems by the PT-symmetric PINN [42]. In this paper, we learn data-driven solutions of the nonlocal SS equation (1) by applying the PINN approach. And comparing the predicted dynamic with the exact dynamic, the validity of the PINN method is illustrated.

The outline of this paper is given as follows. In Sect. 2, the nonlocal integrable SS hierarchies are constructed with the zero curvature equation, which can derive a novel one-component nonlocal SS equation and a novel two-component nonlocal SS system. In addition, the Liouville integrability of the nonlocal integrable SS hierarchies is analyzed by introducing bi-Hamiltonian structures. In Sect. 3, the matrix Riemann-Hilbert problem is established by the analytic and asymptotic properties of the Jost matrix. Then we study a variety of significant symmetry properties of matrix function, scattering matrix, and discrete scattering data of the nonlocal SS equation (1). In Sect. 4, the expressions of N-soliton solutions are given via the Riemann-Hilbert method and symmetry conditions. Then, the dynamic behaviors of one- and two-solion solutions are described in the figures. In Sect. 5, the data-driven solutions of the nonlocal SS equation are learned through the PINN algorithm, which are compared with the exact solutions. Finally, the conclusions of the whole paper are given in Sect. 6.

2 The nonlocal integrable Sasa-Satsuma hierarchies

It can be noted that the multi-component nonlocal integrable hierarchies are derived by the zero curvature equation, thus firstly we show the Lax pair as the following form

$$Y_x = iUY = MY, \quad Y_t = iVY = NY. \tag{7}$$

Then it is natural to give the zero curvature equation based on the above Lax pair

$$M_t - N_x + [M, N] = 0, \tag{8}$$

which is equivalent to $U_t - V_x + i[U, V] = 0$. Furthermore, the spatial part of the Lax pair is introduced below for obtaining multi-component nonlocal integrable SS hierarchies,

$$\begin{aligned} &Y_x = MY = M(\boldsymbol{q}, \boldsymbol{q}^*(-x,-t), z)Y, \\ &M = \begin{pmatrix} izI_{4n} & \boldsymbol{q} \\ -\boldsymbol{q}^*(-x,-t)^\top & -iz \end{pmatrix}, \end{aligned} \tag{9}$$

where $*$ and $\top$ represent the conjugate and the transpose respectively, M is a $(4n+1)$-order matrix, and $\boldsymbol{q}$ denotes a $4n$-dimensional vector potential function

$$\begin{aligned} \boldsymbol{q} = (&q_1, q_1^*, q_1(-x,-t), q_1^*(-x,-t), ..., q_n, \\ &q_n^*, q_n(-x,-t), q_n^*(-x,-t))^\top. \end{aligned} \tag{10}$$

The corresponding stationary zero curvature equation is introduced as

$$\begin{aligned} &N_x = [M,\ N], \quad N = N(\boldsymbol{q}, \boldsymbol{q}^*(-x,-t), z), \\ &M = M(\boldsymbol{q}, \boldsymbol{q}^*(-x,-t), z), \end{aligned} \tag{11}$$

which has a $(4n+1)$-order matrix solution

$$N = \begin{pmatrix} A & B \\ C & D \end{pmatrix} = \sum_{i=0}^{\infty} N_i z^{-i}, \quad N_i = \begin{pmatrix} A^{[i]} & B^{[i]} \\ C^{[i]} & D^{[i]} \end{pmatrix} \tag{12}$$

It is worth mentioning that N_i is independent of z, in which $A^{[i]}$ is a $4n \times 4n$ matrix, $D^{[i]}$ is a 1×1 matrix, and

$$\begin{aligned} &B^{[i]} = (B_1^{[i]}, B_2^{[i]}, ..., B_{4n}^{[i]})^\top, \\ &C^{[i]} = (C_1^{[i]}, C_2^{[i]}, ..., C_{4n}^{[i]}), \quad i \geq 0. \end{aligned} \tag{13}$$

Substitute the expression (12) into the stationary zero curvature formula (11), then a set of matrix equations of A, B, C and D are

$$\begin{cases} A_x = \boldsymbol{q}C + B\boldsymbol{q}^*(-x,-t)^\top, \\ B_x = 2izB + \boldsymbol{q}D - A\boldsymbol{q}, \\ C_x = -2izC - \boldsymbol{q}^*(-x,-t)^\top A + D\boldsymbol{q}^*(-x,-t)^\top, \\ D_x = -\boldsymbol{q}^*(-x,-t)^\top B - C\boldsymbol{q}. \end{cases} \tag{14}$$

The recursion relations of $A^{[i]}$, $B^{[i]}$, $C^{[i]}$ and $D^{[i]}$ are given as

$$\begin{cases} A_x^{[0]} = 0, \quad A_x^{[i]} = \boldsymbol{q}C^{[i]} + B^{[i]}\boldsymbol{q}^*(-x,-t)^\top, \quad i \geq 1, \\ B^{[0]} = 0, \quad B^{[i+1]} = -\frac{i}{2}B_x^{[i]} + \frac{i}{2}\boldsymbol{q}D^{[i]} - \frac{i}{2}A^{[i]}\boldsymbol{q}, \quad i \geq 0, \\ C^{[0]} = 0, \quad C^{[i+1]} = \frac{i}{2}C_x^{[i]} + \frac{i}{2}\boldsymbol{q}^*(-x,-t)^\top A^{[i]} \\ -\frac{i}{2}D^{[i]}\boldsymbol{q}^*(-x,-t)^\top, \quad i \geq 0, \\ D_x^{[0]} = 0, \quad D_x^{[i]} = -\boldsymbol{q}^*(-x,-t)^\top B^{[i]} - C^{[i]}\boldsymbol{q}, \quad i \geq 1. \end{cases} \tag{15}$$

In this case, the first terms of $A^{[i]}$ and $B^{[i]}$ in the recursive expressions can be taken as

$$A^{[0]} = \alpha_1 I_{4n}, \quad D^{[0]} = \alpha_2, \tag{16}$$

where α_1 and α_2 are arbitrary constants. After a series of calculations, it is precise to derive that

$$
\begin{aligned}
A^{[4]} &= \frac{1}{16}\alpha(\boldsymbol{q}\boldsymbol{q}^*(-x,-t)^\top)_{xx} - \frac{3}{16}\alpha\boldsymbol{q}_x\boldsymbol{q}_x^*(-x,-t)^\top \\
&+ \frac{i}{8}\beta(\boldsymbol{q}_x\boldsymbol{q}^*(-x,-t)^\top - \boldsymbol{q}\boldsymbol{q}_x^*(-x,-t)^\top) \\
&+ \frac{3}{16}\alpha(\boldsymbol{q}\boldsymbol{q}^*(-x,-t)^\top\boldsymbol{q}\boldsymbol{q}^*(-x,-t)^\top) \\
&- \frac{1}{4}\gamma\boldsymbol{q}\boldsymbol{q}^*(-x,-t)^\top + \alpha_9 I_{4n}, \\
B^{[4]} &= \frac{1}{16}\alpha\boldsymbol{q}_{xxx} + \frac{i}{8}\beta\boldsymbol{q}_{xx} \\
&+ \frac{3}{16}\alpha\boldsymbol{q}_x\boldsymbol{q}^*(-x,-t)^\top\boldsymbol{q} \\
&+ \frac{3}{16}\alpha\boldsymbol{q}\boldsymbol{q}^*(-x,-t)^\top\boldsymbol{q}_x \\
&- \frac{1}{4}\gamma\boldsymbol{q}_x - \frac{i}{2}\zeta\boldsymbol{q} + \frac{i}{4}\beta\boldsymbol{q}\boldsymbol{q}^*(-x,-t)^\top\boldsymbol{q}, \\
C^{[4]} &= \frac{3}{16}\alpha\boldsymbol{q}^*(-x,-t)^\top\boldsymbol{q}\boldsymbol{q}_x^*(-x,-t)^\top - \frac{1}{4}\gamma\boldsymbol{q}_x^*(-x,-t)^\top \\
&- \frac{i}{4}\beta\boldsymbol{q}^*(-x,-t)^\top\boldsymbol{q}\boldsymbol{q}^*(-x,-t)^\top \\
&+ \frac{1}{16}\alpha\boldsymbol{q}_{xxx}^*(-x,-t)^\top - \frac{i}{8}\beta\boldsymbol{q}_{xx}^*(-x,-t)^\top \\
&+ \frac{3}{16}\alpha\boldsymbol{q}_x^*(-x,-t)^\top\boldsymbol{q}\boldsymbol{q}^*(-x,-t)^\top \\
&+ \frac{i}{2}\zeta\boldsymbol{q}^*(-x,-t)^\top, \\
D^{[4]} &= -\frac{1}{16}\alpha(\boldsymbol{q}^*(-x,-t)^\top\boldsymbol{q})_{xx} + \frac{3}{16}\alpha\boldsymbol{q}_x^*(-x,-t)^\top\boldsymbol{q}_x \\
&+ \frac{i}{8}\beta(\boldsymbol{q}_x^*(-x,-t)^\top\boldsymbol{q} - \boldsymbol{q}^*(-x,-t)^\top \\
&\boldsymbol{q}_x) - \frac{3}{16}\alpha\boldsymbol{q}^*(-x,-t)^\top\boldsymbol{q}\boldsymbol{q}^*(-x,-t)^\top\boldsymbol{q} \\
&+ \frac{1}{4}\gamma\boldsymbol{q}^*(-x,-t)^\top\boldsymbol{q} + \alpha_{10},
\end{aligned}
$$

where α, β, γ, ζ, α_9 and α_{10} are arbitrary constants. According to recursive relations (15), the matrix expression can be written as

$$
\begin{pmatrix} B^{[i+1]} \\ C^{[i+1]\top} \end{pmatrix} = \Gamma \begin{pmatrix} B^{[i]} \\ C^{[i]\top} \end{pmatrix}, \quad i \geq 0, \tag{17}
$$

where Γ is an $(8n \times 8n)$-dimensional matrix integral-differential operator

$$
\Gamma = -\frac{i}{2}\begin{pmatrix} \partial_x + \boldsymbol{q}\partial_x^{-1}\boldsymbol{q}^*(-x,-t)^\top + \sum_{j=1}^{n} h_j & \boldsymbol{q}\partial_x^{-1}\boldsymbol{q}^\top + (\boldsymbol{q}\partial_x^{-1}\boldsymbol{q}^\top)^\top \\ -\boldsymbol{k}(-x,-t)^\top - \boldsymbol{k}(-x,-t) & -\partial_x - \sum_{j=1}^{n} h_j - \boldsymbol{q}^*(-x,-t)^\top\partial_x^{-1}\boldsymbol{q}^\top \end{pmatrix}, \tag{18}
$$

in which

$$
\begin{aligned}
h_j &= q_j\partial_x^{-1}q_j^*(-x,-t)^\top + q_j^*(-x,-t)^\top\partial_x^{-1}q_j, \\
\boldsymbol{k}(-x,-t) &= \boldsymbol{q}^*(-x,-t)^\top\partial_x^{-1}\boldsymbol{q}^*(-x,-t).
\end{aligned}
$$

Then, the jth evolution equation of temporal spectral matrix in the hierarchy is introduced as follows

$$
\begin{aligned}
N^{[j]} &= N^{[j]}(\boldsymbol{q}, \boldsymbol{q}^*(-x,-t), z) = (z^j N)_+ \\
&= \sum_{i=0}^{j} N_i z^{j-i}, \ j \geq 1.
\end{aligned} \tag{19}
$$

Combining with the zero curvature formula $M_{t_j} - N_x^{[j]} + [M, N^{[j]}] = 0, \ j \geq 1$, the nonlocal integrable SS hierarchies are obtained as

$$
\begin{pmatrix} \boldsymbol{q}_{t_j} \\ \boldsymbol{q}_{t_j}^*(-x,-t) \end{pmatrix} = 2i\begin{pmatrix} B^{[j+1]} \\ C^{[j+1]\top} \end{pmatrix}, \quad j \geq 1. \tag{20}
$$

When $j = 3$, we suppose these functions subject to $q_2 = q_3 = 0$ and take the constants $\alpha = 8i$, $\beta = \gamma = \zeta = 0$. The one-component nonlocal SS equation is given according to the above nonlocal integrable hierarchies (20),

$$
\begin{aligned}
&q_{1,t_3} + q_{1,xxx} + 6(q_1q_1^*(-x,-t) + q_1(-x,-t)q_1^*)q_{1x} \\
&+3q_1(q_1q_1^*(-x,-t) + q_1^*q_1(-x,-t))_x = 0.
\end{aligned} \tag{21}
$$

Similarly, supposing the function $q_3 = 0$, the two-component nonlocal SS system is obtained

$$
\begin{aligned}
&q_{1,t_3} + q_{1,xxx} + 6(q_1q_1^*(-x,-t) + q_1(-x,-t)q_1^*)q_{1x} \\
&+ 3q_1(q_1q_1^*(-x,-t) + q_1^*q_1(-x,-t))_x = 0, \\
&q_{2,t_3} + q_{2,xxx} + 6(q_2q_2^*(-x,-t) + q_2(-x,-t)q_2^*)q_{2x} \\
&+ 3q_2(q_2q_2^*(-x,-t) + q_2^*q_2(-x,-t))_x = 0.
\end{aligned} \tag{22}
$$

In order to investigate the Liouville integrability [43] for nonlocal integrable SS hierarchies (20), the bi-Hamiltonian structures [44,45] are introduced from the trace identity. Firstly, the conditions satisfied by the traces are given

$$
\operatorname{tr}\left(N\frac{\partial M}{\partial z}\right) = i[\operatorname{tr}(A) - D]
$$

$$= i\left[\sum_{i=0}^{\infty}\left(\sum_{j=1}^{4n} A_{jj}^{[i]} - D^{[i]}\right) z^{-i}\right], \tag{23}$$

$$\operatorname{tr}\left(N\frac{\partial M}{\partial \boldsymbol{q}}\right) \tag{24}$$

$$= \begin{pmatrix} C^{\top} \\ -B \end{pmatrix} = \sum_{i=0}^{\infty}\begin{pmatrix} C^{[i]\top} \\ -B^{[i]} \end{pmatrix} z^{-i} = \sum_{i=0}^{\infty} G_{i-1} z^{-i}.$$

Then, learning from the trace identity and the variational identity, we know

$$\frac{\delta \tilde{H}_i}{\delta \boldsymbol{q}} = iG_{i-1}, \quad \tilde{H}_i = i\int\left(\sum_{j=1}^{4n} A_{jj}^{[i+1]} - D^{[i+1]}\right) dx/i. \tag{25}$$

It can thus be seen that bi-Hamiltonian structures for the nonlocal integrable SS hierarchies (20) are introduced as

$$\begin{pmatrix} \boldsymbol{q}_{t_i} \\ \boldsymbol{q}^*_{t_i}(-x,-t) \end{pmatrix} = J_1\frac{\delta \tilde{H}_{i+1}}{\delta \boldsymbol{q}} = J_2\frac{\delta \tilde{H}_i}{\delta \boldsymbol{q}}, \quad i \geq 1, \tag{26}$$

where

When $x \to \pm\infty$ or $t \to \pm\infty$, the potential function q is assumed to decay sufficiently rapidly to zero. From the above differential equation (28), the Y could be expressed as

$$Y = Je^{iz\Lambda x + 4iz^3\Lambda t}, \tag{29}$$

where the matrix function J satisfies these differential equations

$$J_x = iz[\Lambda, J] + Q_1 J, \quad J_t = 4iz^3[\Lambda, J] + P_1 J. \tag{30}$$

Then matrix eigenfunctions $J_+(x,t)$ and $J_-(x,t)$ are introduced with asymptotic properties

$$J_{\pm}(x,t) \to I_5, \quad x \to \pm\infty, \tag{31}$$

where the subscript $\pm$ indicates that the asymptotic boundary is at the positive or negative end of the x-axis, and determinants of J_+ and J_- are both one. So as to facilitate the analysis for properties of eigenfunctions, we suppose a notation $E = e^{iz\Lambda x}$ and

$$J_1 = \begin{pmatrix} 0 & -2I_{4n} \\ 2I_{4n} & 0 \end{pmatrix},$$

$$J_2 = i\begin{pmatrix} -\boldsymbol{q}\partial_x^{-1}\boldsymbol{q}^{\top} - (\boldsymbol{q}\partial_x^{-1}\boldsymbol{q}^{\top})^{\top} & \partial_x + \boldsymbol{q}\partial_x^{-1}\boldsymbol{q}^*(-x,-t)^{\top} + \sum_{j=1}^{n} h_j \\ \partial_x + \sum_{j=1}^{n} h_j + \boldsymbol{q}^*(-x,-t)^{\top}\partial_x^{-1}\boldsymbol{q}^{\top} & -\boldsymbol{k}(-x,-t)^{\top} - \boldsymbol{k}(-x,-t) \end{pmatrix}.$$

Thus, the nonlocal integrable SS hierarchies (20) are decomposed into two commuting finite-dimensional Hamiltonian systems being Liouville integrable. Moreover, the integrable property of one-component or multi-component nonlocal SS systems is illustrated.

3 Riemann-Hilbert problem for the nonlocal Sasa-Satsuma equation

In this section, the Riemann-Hilbert problem for the nonlocal SS equation (1) is accurately constructed, which can help us to analyze the general soliton solutions. Based on Lax pair (2) and concrete expressions of U and V, we take

$$Q_1 = iQ, \quad P_1 = iP, \tag{27}$$

thus,

$$Y_x = iz\Lambda Y + Q_1 Y, \quad Y_t = 4iz^3\Lambda Y + P_1 Y. \tag{28}$$

$$\Phi_- = J_- E, \quad \Phi_+ = J_+ E. \tag{32}$$

Notice that Φ_+ and Φ_- are the eigenfunctions of the spatial spectrum problem in (28), thus there is a linear correlation between Φ_- and Φ_+

$$\Phi_- = \Phi_+ S(z) \Longleftrightarrow J_- E = J_+ E S(z), \quad z \in \mathbb{R}, \tag{33}$$

where the scattering matrix $S(z) = (s_{jl})_{5\times 5}$. Since the determinants of J_+ and J^- are both one, the matrix determinant of $S(z)$ is also one. It is worth mentioning that the eigenfunctions $J_{\pm}(x,z)$ satisfying the spatial matrix spectrum problem in (30) are given as these Volterra integral expressions

$$J_-(x,z) = I_5 + \int_{-\infty}^{x} e^{iz\Lambda(x-y)} Q_1(y) J_-(y,z) e^{-iz\Lambda(x-y)} dy, \tag{34}$$

$$J_+(x,z) = I_5 + \int_{+\infty}^{x} e^{iz\Lambda(x-y)} Q_1(y) J_+(y,z) e^{-iz\Lambda(x-y)} dy. \tag{35}$$

Just to make it easier to represent each column vector of $J_\pm(x,z)$, the notation is introduced as

$$J_\pm(x,z) = (J_{\pm,1}, J_{\pm,2}, J_{\pm,3}, J_{\pm,4}, J_{\pm,5}). \tag{36}$$

Through analyzing the convergence of the Volterra integrals in (34) and (35), $J_{+,i}$ $(i = 1,2,3,4)$ and $J_{-,5}$ possess analyticity on region $\mathbb{C}_+$ and continuity on region $\bar{\mathbb{C}}_+$. In the meantime, $J_{+,5}$ and $J_{-,i}$ $(i = 1,2,3,4)$ satisfy analyticity on region $\mathbb{C}_-$ and continuity on region $\bar{\mathbb{C}}_-$. Then, we construct the Jost solution Ψ^+ which has analytic property in $\mathbb{C}_+$ and continuous property in $\bar{\mathbb{C}}_+$,

$$\begin{aligned}\Psi^+ &= \Psi^+(x,z) = (J_{+,1}, J_{+,2}, J_{+,3}, J_{+,4}, J_{-,5})\\ &= J_- H_1 + J_+ H_2,\end{aligned} \tag{37}$$

where

$$H_1 = \mathrm{diag}(0,0,0,0,1)_{5\times5},\ \ H_2 = \mathrm{diag}(1,1,1,1,0)_{5\times5}. \tag{38}$$

Similarly, the next is to obtain the matrix Jost solution Ψ^- with the lower half plane analysis, which means that Ψ^- possesses analytic property in $\mathbb{C}_-$. Unlike above, we need to consider the adjoint matrix equations of (2) and (30), respectively,

$$i\tilde{Y}_x = \tilde{Y}U, \quad i\tilde{Y}_t = \tilde{Y}V, \tag{39}$$

$$i\tilde{J}_x = z[\tilde{J},\Lambda] + \tilde{J}Q, \quad i\tilde{J}_t = 4z^3[\tilde{J},\Lambda] + \tilde{J}P. \tag{40}$$

The eigenfunctions of the above adjoint matrix equations are obtained as

$$\tilde{Y}_\pm = (Y_\pm)^{-1}, \quad \tilde{J}_\pm = (J_\pm)^{-1}, \tag{41}$$

and the eigenfunctions $\tilde{J}_\pm(x,z)$ could be defined as

$$\tilde{J}_\pm(x,z) = (\tilde{J}_{\pm,1}, \tilde{J}_{\pm,2}, \tilde{J}_{\pm,3}, \tilde{J}_{\pm,4}, \tilde{J}_{\pm,5})^\top, \tag{42}$$

where $\tilde{J}_{\pm,i}$ represent the ith row vectors of the eigenfunctions $\tilde{J}_\pm$. Then, the matrix Jost solution Ψ^- with the lower half plane analysis is constructed as follows

$$\begin{aligned}\Psi^-(x,z) &= (\tilde{J}_{+,1}, \tilde{J}_{+,2}, \tilde{J}_{+,3}, \tilde{J}_{+,4}, \tilde{J}_{-,5})^\top\\ &= H_1\tilde{J}_- + H_2\tilde{J}_+ = H_1(J_-)^{-1} + H_2(J_+)^{-1}.\end{aligned} \tag{43}$$

In view of linear relationship (33) between J_- and J_+ and the expressions (37) and (43) of $\Psi^\pm(x,z)$, the determinants of Ψ^+ and Ψ^- are calculated as

$$\det\Psi^+(x,z) = s_{55}(z), \quad \det\Psi^-(x,z) = \hat{s}_{55}(z), \tag{44}$$

and the limits of Ψ^+ and Ψ^- as x approaches infinity are obtained as

$$\lim_{x\to\infty}\Psi^+(x,z) = \begin{pmatrix} I_4 & 0\\ 0 & s_{55}(z)\end{pmatrix}, \quad z\in\bar{\mathbb{C}}_+, \tag{45}$$

$$\lim_{x\to\infty}\Psi^-(x,z) = \begin{pmatrix} I_4 & 0\\ 0 & \hat{s}_{55}(z)\end{pmatrix}, \quad z\in\bar{\mathbb{C}}_-, \tag{46}$$

where $\hat{s}_{55}(z)$ is the fifth row and fifth column element of the inverse scattering matrix $S^{-1}(z)$, and $S^{-1}(z) = (\hat{s}_{ij})_{5\times5}$. Thus, the Jost matrixes $G^+(x,z)$ and $G^-(x,z)$ are constructed as follows

$$G^+(x,z) = \Psi^+(x,z)\begin{pmatrix} I_4 & 0\\ 0 & s_{55}^{-1}(z)\end{pmatrix}, \quad z\in\bar{\mathbb{C}}_+, \tag{47}$$

$$G^-(x,z) = \begin{pmatrix} I_4 & 0\\ 0 & \hat{s}_{55}^{-1}(z)\end{pmatrix}\Psi^-(x,z), \quad z\in\bar{\mathbb{C}}_-, \tag{48}$$

which both asymptotically approach the identity matrix as $x\to\infty$.

Proposition 3.1 *Based on the definitions of $G^\pm(x,z)$, the matrix Riemann-Hilbert problem satisfies*

i) the relationship between $G^+(x,z)$ and $G^-(x,z)$

$$G^-(x,z)G^+(x,z) = G_0(x,z), \quad z\in\mathbb{R}, \tag{49}$$

where

$$\begin{aligned}G_0(x,z) &= E\begin{pmatrix} I_4 & 0\\ 0 & \hat{s}_{55}^{-1}\end{pmatrix}\\ &(H_1S^{-1}+H_2)(SH_1+H_2)\begin{pmatrix} I_4 & 0\\ 0 & s_{55}^{-1}\end{pmatrix}E^{-1}\\ &= E\begin{pmatrix} I_4 & 0\\ 0 & \hat{s}_{55}^{-1}\end{pmatrix}\begin{pmatrix} 1 & 0 & 0 & 0 & s_{15}\\ 0 & 1 & 0 & 0 & s_{25}\\ 0 & 0 & 1 & 0 & s_{35}\\ 0 & 0 & 0 & 1 & s_{45}\\ \hat{s}_{51} & \hat{s}_{52} & \hat{s}_{53} & \hat{s}_{54} & 1\end{pmatrix}\begin{pmatrix} I_4 & 0\\ 0 & s_{55}^{-1}\end{pmatrix}E^{-1}.\end{aligned} \tag{50}$$

ii) $G^+(x,z)\to I_5$, $z\in\mathbb{C}_+\to\infty$.
iii) $G^-(x,z)\to I_5$, $z\in\mathbb{C}_-\to\infty$.

It is vital to derive symmetric relations of matrix functions, Jost matrices, scattering matrix and discrete scattering data, which are preliminary preparations for obtaining soliton solutions. Thus, we analyze these symmetry constraints of the nonlocal SS equation (1). Firstly, the symmetric properties of matrixes Q and P need to take into account

$$Q^\dagger(-x,-t) = Q(x,t), \quad P^\dagger(-x,-t) = P(x,t), \tag{51}$$

where the notation $\dagger$ denotes the Hermitian (i.e. conjugate transpose) of a matrix. In view of the adjoint matrix equation (40) with the eigenfunction J^{-1}, the symmetric relation for the function J is shown as

$$J^\dagger(-x,-t,-z^*) = J^{-1}(x,t,z). \tag{52}$$

This illustrates $J^{\dagger}(-x,-t,-z^*)$ is also a solution of the adjoint matrix spectrum problem (40), and both z and $-z^*$ are the eigenvalues of spectrum problems (30) and (40). According to the expression $E=e^{iz\Lambda x}$ and the linear correlation (33) between J_- and J_+, there are

$$E^{\dagger}(-x,-t,-z^*)=E^{-1}(x,t,z), \tag{53}$$
$$S^{\dagger}(-z^*)=S^{-1}(z), \tag{54}$$

thus, $s_{55}^*(-z^*)=\hat{s}_{55}(z)$. Then, combining with the definitions (37) and (43) of Ψ^+ and Ψ^-, the symmetric constraint between Ψ^+ and Ψ^- is

$$(\Psi^+)^{\dagger}(-x,-z^*)=\Psi^-(x,z). \tag{55}$$

4 N-soliton solutions of the nonlocal equation and their dynamics

On the basis of known Riemann-Hilbert problem and symmetric conditions, the N-soliton solutions of the nonlocal SS equation (1) and their dynamic features are investigated in this section. Firstly, in order to analyze the relation between the solution q and the Jost solution G^+, the asymptotic expansion of G^+ is supposed as

$$\begin{aligned}G^+(x,t,z)&=I_5+z^{-1}G_1^+(x,t)\\&+z^{-2}G_2^+(x,t)+O(z^{-3}),\quad z\to\infty,\end{aligned} \tag{56}$$

which satisfies

$$G_x^+(x,t,z)=iz[\Lambda,G^+(x,t,z)]+Q_1G^+(x,t,z) \tag{57}$$

Thus, $Q_1=-i[\Lambda,G_1^+(x,t)]$ is equivalent to $Q=-[\Lambda,G_1^+(x,t)]$, and then the following equations are true

$$\begin{aligned}q(x,t)&=-2i(G_1^+)_{15}=-2i(G_1^+)_{54},\\q(-x,-t)&=-2i(G_1^+)_{35}=-2i(G_1^+)_{52},\end{aligned} \tag{58}$$
$$\begin{aligned}q^*(x,t)&=-2i(G_1^+)_{25}=-2i(G_1^+)_{53},\\q^*(-x,-t)&=-2i(G_1^+)_{45}=-2i(G_1^+)_{51},\end{aligned} \tag{59}$$

where $(G_1^+)_{ij}$ is the element of the matrix G_1^+ in row i and column j.

Based on the above determinants of Jost matrices $\Psi^{\pm}$ and the symmetry property for scattering matrix S, z_k is the zero of $\det\Psi^+(x,z)$, then $-z_k^*$ is also the zero of $\det\Psi^+(x,z)$ and $\hat{z}_k=z_k^*$ is the zero of $\det\Psi^-(x,z)$. Accordingly, the expressions for the kernels of $\Psi^+(z_k)$ and $\Psi^-(\hat{z}_k)$ are shown as

$$\Psi^+(z_k)v_k=0,\quad \hat{v}_k\Psi^-(\hat{z}_k)=0, \tag{60}$$

where the kernel v_k is a nonzero column vector and the kernel $\hat{v}_k$ is a nonzero row vector. As well as we know, $\Psi^+(z_k)$ is the solution of differential equations (30), thus, v_k satisfies

$$\begin{aligned}&(v_k)_x=iz_k\Lambda v_k,\ (v_k)_t=4iz_k^3\Lambda v_k,\ \Rightarrow\\&v_k=v_k(x,t,z_k)=e^{iz_k\Lambda x+4iz_k^3\Lambda t}w_k,\end{aligned} \tag{61}$$

where w_k is an arbitrary column vector, and it may as well be assumed to $(a_k,b_k,c_k,d_k,1)^{\top}$. According to the symmetric constraint (55) between Ψ^+ and Ψ^-, the expression of $\hat{v}_k$ is derived as

$$\begin{aligned}\hat{v}_k&=\hat{v}_k(x,t,\hat{z}_k)=v_k^{\dagger}(-x,-t,-z_k)\\&=w_k^{\dagger}e^{-iz_k^*\Lambda x-4iz_k^{*3}\Lambda t}.\end{aligned} \tag{62}$$

In view of Riemann-Hilbert problem constructed above and containing analytical solution as $G_0=I$, the solution $G^+(x,t,z)$ of this sort of Riemann-Hilbert problem is

$$G^+(x,t,z)=I_5-\sum_k\sum_l\frac{v_k(M^{-1})_{kl}\hat{v}_l}{z-\hat{z}_k}, \tag{63}$$

where $M=(m_{kl})_{n\times n}$, and $m_{kl}=\frac{\hat{v}_kv_l}{z_l-\hat{z}_k}$, $(z_l\neq\hat{z}_k)$.

For the number of zeros of $\det\Psi^{\pm}(x,z)$, there are two cases discussed in the following. In the first case, the determinant of $\Psi^+(x,z)$ obtains $2N$ zeros $z_k\in\mathbb{C}_+$ $(1\le k\le 2N)$, which satisfy $z_{N+k}=-z_k^*$ $(1\le k\le N)$. Correspondingly, the determinant of $\Psi^-(x,z)$ contains $2N$ zeros $\hat{z}_k\in\mathbb{C}_-$ $(1\le k\le 2N)$, which satisfy $\hat{z}_k=z_k^*$ $(1\le k\le 2N)$. Combining the asymptotic expansion (56) with the expression (63) of G^+, we know

$$G_1^+(x,t)=-\sum_{k,l=1}^{2N}v_k(M^{-1})_{kl}\hat{v}_l. \tag{64}$$

Through calculation, the one-soliton solution of the nonlocal SS equation (1) can be obtained from (58) as

$$\begin{aligned}q=2i(&e^{\theta_1-\theta_1^*}a_1(M^{-1})_{11}+e^{\theta_1-\theta_2^*}a_1(M^{-1})_{12}\\&+e^{\theta_2-\theta_1^*}a_2(M^{-1})_{21}+e^{\theta_2-\theta_2^*}a_2(M^{-1})_{22}),\end{aligned} \tag{65}$$

where $q=q(x,t)$, $\theta_k=iz_kx+4iz_k^3t$ $(k=1,2)$, $M=(m_{kl})_{2\times 2}$, and

$$\begin{aligned}m_{11}&=(e^{\theta_1+\theta_1^*}(|a_1|^2+|b_1|^2+|c_1|^2+|d_1|^2)\\&\quad+e^{-\theta_1-\theta_1^*})/(z_1-z_1^*),\\m_{12}&=(e^{\theta_1^*+\theta_2}(a_1^*a_2+b_1^*b_2+c_1^*c_2+d_1^*d_2)\\&\quad+e^{-\theta_1^*-\theta_2})/(z_2-z_1^*),\end{aligned}$$

$$m_{21} = (e^{\theta_1+\theta_2^*}(a_2^*a_1 + b_2^*b_1 + c_2^*c_1 + d_2^*d_1) \\ +e^{-\theta_1-\theta_2})/(z_1 - z_2^*),$$

$$m_{22} = (e^{\theta_2+\theta_2^*}(|a_2|^2 + |b_2|^2 + |c_2|^2 + |d_2|^2) \\ +e^{-\theta_2-\theta_2^*})/(z_2 - z_2^*).$$

Since $z_2 = -z_1^*$ and $v_2 = v_1^*$, these are true with $\theta_2 = \theta_1^*$ and $(a_2, b_2, c_2, d_2, 1) = (a_1^*, b_1^*, c_1^*, d_1^*, 1)$. When $N = 2$, the two-soliton solution of the nonlocal SS equation (1) can be derived from (58) as follows

$$\begin{aligned} q =& 2i(e^{\theta_1-\theta_1^*}a_1(M^{-1})_{11} + e^{\theta_1-\theta_2^*}a_1(M^{-1})_{12} \\ &+ e^{\theta_1-\theta_3^*}a_1(M^{-1})_{13} + e^{\theta_1-\theta_4^*}a_1(M^{-1})_{14} \\ &+ e^{\theta_2-\theta_1^*}a_2(M^{-1})_{21} + e^{\theta_2-\theta_2^*}a_2(M^{-1})_{22} \\ &+ e^{\theta_2-\theta_3^*}a_2(M^{-1})_{23} + e^{\theta_2-\theta_4^*}a_2(M^{-1})_{24} \\ &+ e^{\theta_3-\theta_1^*}a_3(M^{-1})_{31} + e^{\theta_3-\theta_2^*}a_3(M^{-1})_{32} \\ &+ e^{\theta_3-\theta_3^*}a_3(M^{-1})_{33} + e^{\theta_3-\theta_4^*}a_3(M^{-1})_{34} \\ &+ e^{\theta_4-\theta_1^*}a_4(M^{-1})_{41} + e^{\theta_4-\theta_2^*}a_4(M^{-1})_{42} \\ &+ e^{\theta_4-\theta_3^*}a_4(M^{-1})_{43} + e^{\theta_4-\theta_4^*}a_4(M^{-1})_{44}), \end{aligned} \tag{66}$$

where $M = (m_{kl})_{4\times4}$, and $m_{kl} = (e^{\theta_l+\theta_k^*}(a_la_k^* + b_lb_k^* + c_lc_k^* + d_ld_k^*) + e^{-\theta_l-\theta_k^*})/(z_l - z_k^*)$. Similarly, there are $\theta_3 = \theta_1^*$, $\theta_4 = \theta_2^*$, $(a_3, b_3, c_3, d_3, 1) = (a_1^*, b_1^*, c_1^*, d_1^*, 1)$ and $(a_4, b_4, c_4, d_4, 1) = (a_2^*, b_2^*, c_2^*, d_2^*, 1)$.

Some figures, such as Fig. 1 and Fig. 2, intuitively show the dynamics of solutions (65) and (66) of the nonlocal SS equation (1). In Fig. 1, there are two images of one-soliton solutions due to the difference in parameter z_1, yet they have the same parameters $(a_1, b_1, c_1, d_1) = (1+0.5i, -1+i, 0.5+i, -2+2i)$. The breather-type of one-soliton solutions in Fig. 1 are periodic waves, i.e. the amplitude and waveshape are unchanged with time. The difference between the two graphical representations of the one-soliton solutions (65) is the spacing of each breather. In the meantime, there are three different images of two-soliton solutions (66), which are shown in Fig. 2 with the same parameters $(a_1, b_1, c_1, d_1) = (1+i, -1+2i, 1+0.5i, 2+i)$ and $(a_2, b_2, c_2, d_2) = (1+i, 2+2i, -1+i, -1+2i)$. In (a)-(d), the waveforms of the two-soliton solutions can be seen as the oblique elastic collision between two breather-type solitons. It is worth mentioning that the difference between the first one and the second one is the direction in which the two breather-type waves collide. In (e)-(f), the waveform consists of the oblique elastic interaction between a line soliton and a breather-type soliton. The propagation velocity and amplitude of these waves before and after the collision remain unchanged.

In the second case, the determinant of $\Psi^+(x, z)$ obtains N pure imaginary zeros $z_k \in \mathbb{C}_+(1 \le k \le N)$, meanwhile, $\hat{z}_k = z_k^* \in \mathbb{C}_-(1 \le k \le N)$ are the zeros of the determinant of $\Psi^-(x, z)$. In this time, the expression of $G_1^+(x, t)$ is given as

$$G_1^+(x, t) = -\sum_{k,l=1}^{N} v_k(M^{-1})_{kl}\hat{v}_l. \tag{67}$$

Then, the N-soliton solutions of the nonlocal SS equation (1) can be calculated from (58) and (59) as

$$\begin{aligned} q(x, t) &= 2i\sum_{k,l=1}^{N} e^{\theta_k-\theta_l^*}a_k(M^{-1})_{kl} \\ &= 2i\sum_{k,l=1}^{N} e^{-\theta_k+\theta_l^*}d_l^*(M^{-1})_{kl}, \end{aligned} \tag{68}$$

$$\begin{aligned} q^*(x, t) &= 2i\sum_{k,l=1}^{N} e^{\theta_k-\theta_l^*}b_k(M^{-1})_{kl} \\ &= 2i\sum_{k,l=1}^{N} e^{-\theta_k+\theta_l^*}c_l^*(M^{-1})_{kl}, \end{aligned} \tag{69}$$

$$\begin{aligned} q(-x, -t) &= 2i\sum_{k,l=1}^{N} e^{\theta_k-\theta_l^*}c_k(M^{-1})_{kl} \\ &= 2i\sum_{k,l=1}^{N} e^{-\theta_k+\theta_l^*}b_l^*(M^{-1})_{kl}, \end{aligned} \tag{70}$$

$$\begin{aligned} q^*(-x, -t) &= 2i\sum_{k,l=1}^{N} e^{\theta_k-\theta_l^*}d_k(M^{-1})_{kl} \\ &= 2i\sum_{k,l=1}^{N} e^{-\theta_k+\theta_l^*}a_l^*(M^{-1})_{kl}, \end{aligned} \tag{71}$$

where $\theta_k = iz_kx + 4iz_k^3t$ $(k = 1, 2, 3..., N)$, $M = (m_{kl})_{N\times N}$. When $N = 1$, the one-soliton solution in this case is

$$q = 2ie^{\theta_1-\theta_1^*}a_1(M^{-1})_{11}, \tag{72}$$

where $M = (m_{kl})_{1\times1}$, and

$$m_{11} = \frac{e^{\theta_1+\theta_1^*}(|a_1|^2 + |b_1|^2 + |c_1|^2 + |d_1|^2) + e^{-\theta_1-\theta_1^*}}{z_1 - z_1^*}, \tag{73}$$

$$(a_1, b_1, c_1, d_1) = \left(\frac{e^{i\gamma_1}}{2}, \frac{e^{i\gamma_1}}{2}, \frac{e^{i\gamma_1}}{2}, \frac{e^{i\gamma_1}}{2}, 1\right), \tag{74}$$

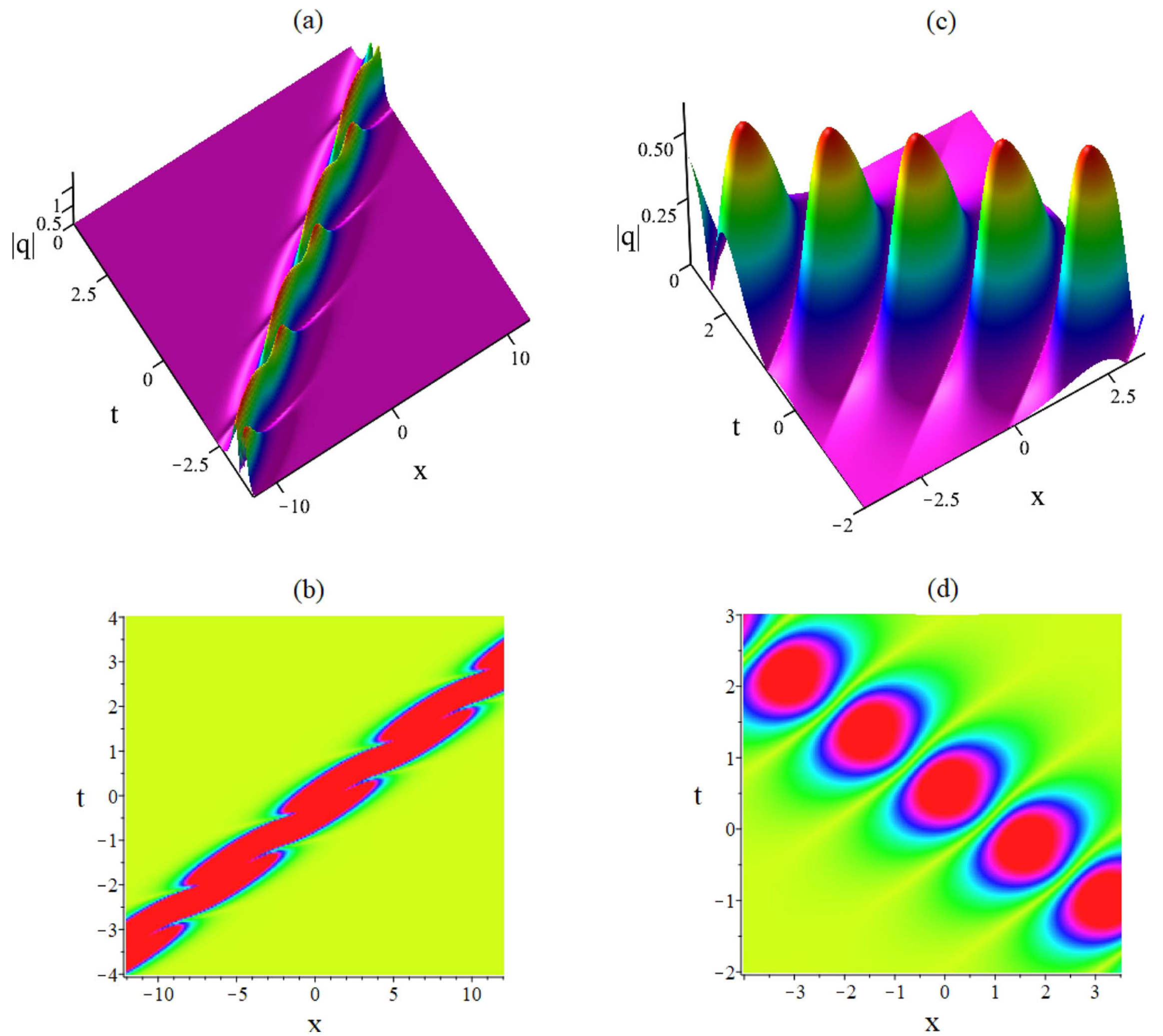

Fig. 1 One-soliton given in (65) of the nonlocal SS equation (1). (a) and (b) with parameter: $z_1 = 0.12 + i$. (c) and (d) with parameter: $z_1 = 0.5 + 0.5i$

and γ_1 is an arbitrary real parameter. So, in like manner, the two-soliton solution in this case is

$$q = 2i(e^{\theta_1-\theta_1^*}a_1(M^{-1})_{11} + e^{\theta_1-\theta_2^*}a_1(M^{-1})_{12} + e^{\theta_2-\theta_1^*}a_2(M^{-1})_{21} + e^{\theta_2-\theta_2^*}a_2(M^{-1})_{22}), \tag{75}$$

where $M = (m_{kl})_{2\times 2}$, and

$$m_{11} = \frac{e^{\theta_1+\theta_1^*}(|a_1|^2 + |b_1|^2 + |c_1|^2 + |d_1|^2) + e^{-\theta_1-\theta_1^*}}{z_1 - z_1^*}, \tag{76}$$

$$m_{12} = \frac{e^{\theta_2+\theta_1^*}(a_1^*a_2 + b_1^*b_2 + c_1^*c_2 + d_1^*d_2) + e^{-\theta_2-\theta_1^*}}{z_2 - z_1^*}, \tag{77}$$

$$m_{21} = \frac{e^{\theta_1+\theta_2^*}(a_1a_2^* + b_1b_2^* + c_1c_2^* + d_1d_2^*) + e^{-\theta_1-\theta_2^*}}{z_1 - z_2^*}, \tag{78}$$

$$m_{22} = \frac{e^{\theta_2+\theta_2^*}(|a_2|^2 + |b_2|^2 + |c_2|^2 + |d_2|^2) + e^{-\theta_2-\theta_2^*}}{z_2 - z_2^*}, \tag{79}$$

$$(a_1, b_1, c_1, d_1) = \left(\frac{e^{i\gamma_1}}{2}, \frac{e^{i\gamma_1}}{2}, \frac{e^{i\gamma_1}}{2}, \frac{e^{i\gamma_1}}{2}, 1\right),$$
$$(a_2, b_2, c_2, d_2) = \left(\frac{e^{i\gamma_2}}{2}, \frac{e^{i\gamma_2}}{2}, \frac{e^{i\gamma_2}}{2}, \frac{e^{i\gamma_2}}{2}, 1\right), \tag{80}$$

and γ_1 and γ_2 are arbitrary real parameters.

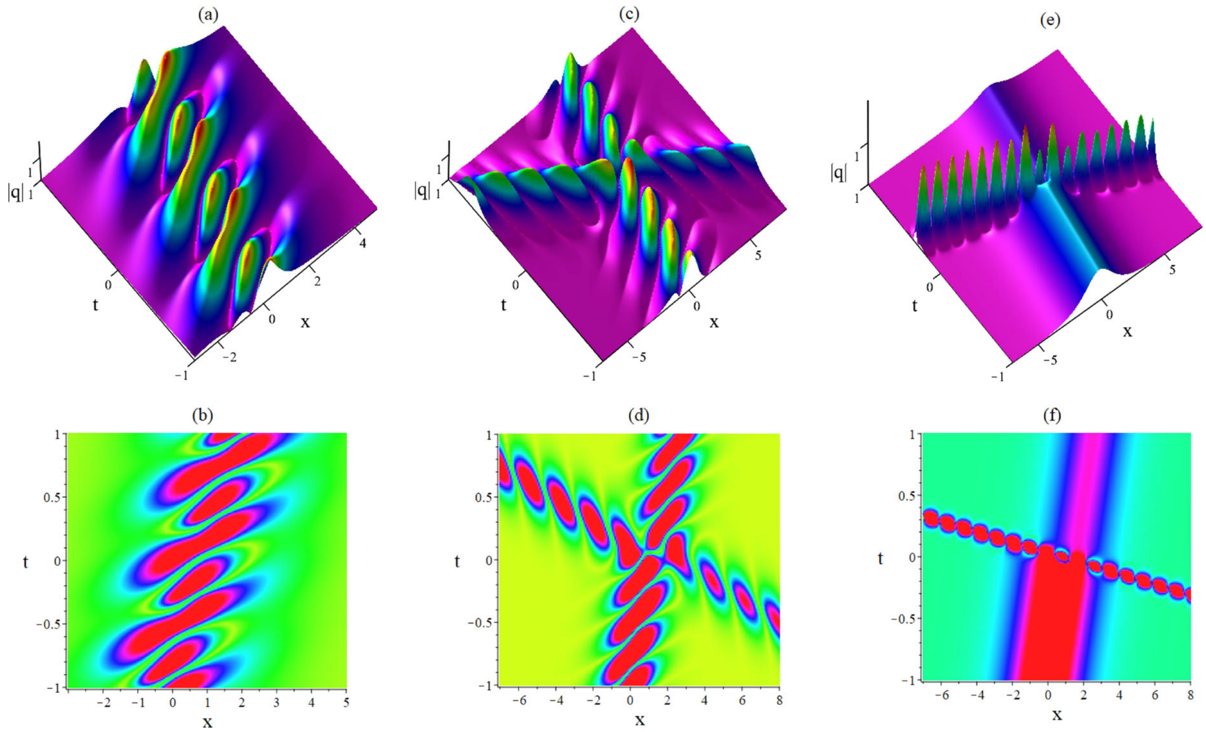

Fig. 2 Two-soliton given in (66) of the nonlocal SS equation (1). (a) and (b) with parameters: $(z_1, z_2) = (0.5i, 0.5 + i)$. (c) and (d) with parameters: $(z_1, z_2) = (0.5 + i, 1 + 0.5i)$. (e) and (f) with parameters: $(z_1, z_2) = (0.5i, 1.5 + i)$

Figure 3 and Fig. 4 respectively present the dynamic characteristics of solutions (72) and (75) in this case. In Fig. 3, one-soliton solution of the nonlocal SS equation (1) has the shape of a line soliton, which is the most common type of waveform among single solitons with a constant amplitude. At the same time, two-soliton solutions of the nonlocal SS equation (1) are displayed in Fig. 4, which presents two different forms. The first one is an oblique elastic collision between a line soliton and a breather-type soliton, and the second one is an oblique elastic collision between two line solitons. It is obvious that the amplitude increases at the moment of the interaction, and the propagation direction of one of the branches changes before and after the collision.

5 The PINN method and the data-driven solutions

In this section, we would like to obtain some data-driven solutions of the nonlocal SS equation (1) by applying the PINN method. Meanwhile, the feasibility of the PINN approach could be analyzed by the experiment. Firstly, give the initial condition and boundary condition of the nonlocal SS equation (1)

$$q(x, t_1) = q_1(x), \ x \in [x_1, x_2], \tag{81}$$

$$q(x_1, t) = q_{lb}(t), \ q(x_2, t) = q_{ub}(t), \ t \in [t_1, t_2]. \tag{82}$$

It is easy to see that the range in the x direction is $[x_1, x_2]$ and in the t direction is $[t_1, t_2]$. Considering the existence of nonlocal terms, and effectively separating the real and imaginary parts of the function expressions, we would like to suppose that $q(x, t) = u(x, t) + iv(x, t)$ and $q^*(-x, -t) = u(-x, -t) - iv(-x, -t)$. Introducing $u = u(x, t)$ and $v = v(x, t)$, the nonlocal SS equation (1) is transformed into

$$\begin{aligned} &u_t + iv_t + u_{xxx} + iv_{xxx} + 12(uu(-x, -t) \\ &+ vv(-x, -t))(u_x + iv_x) + 6(u + iv) \\ &(uu(-x, -t) + vv(-x, -t))_x = 0, \end{aligned} \tag{83}$$

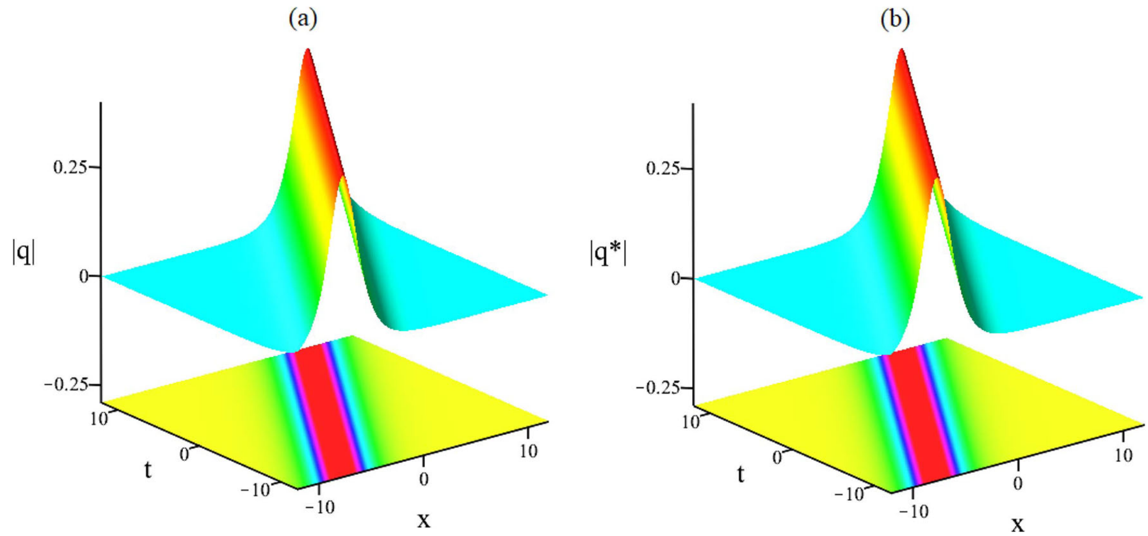

Fig. 3 One-soliton given in (72) of the nonlocal SS equation (1). (a) and (b) with parameters: $z_1 = 0.4i$, γ_1=2

Then, the form of the equation in PINN is obtained by separating the real and imaginary parts, which is given as

$$\begin{cases} f_u := u_t + u_{xxx} + 12(u(-x,-t)u + v(-x,-t)v)u_x \\ \qquad + 6u(u(-x,-t)u + v(-x,-t)v)_x, \\ f_v := v_t + v_{xxx} + 12(u(-x,-t)u + v(-x,-t)v)v_x \\ \qquad + 6v(u(-x,-t)u + v(-x,-t)v)_x. \end{cases} \tag{84}$$

Combining with the weight ω and bias b, the solutions u and v in the above expressions can be applied to simulate the solutions for the nonlocal SS equation, meanwhile, they are the output elements of the PINN. Moreover, the PINN algorithm has a network of L layers, and in addition to the input and output layers, each layer has N_l neurons. And the PINN is a fully connected multi-layer feedforward neural network, in which the relationship between the front and back layers of neurons can be expressed as

$$\boldsymbol{x}^l \triangleq \sigma(W^l \boldsymbol{x}^{l-1} + \boldsymbol{b}^l). \tag{85}$$

To observe the structure of the neural network more intuitively, the frame diagram of the PINN algorithm is displayed in Fig. 5 below. It is obvious that this network not only obtains the part of neural neurons but also contains the part of physical information of the equation, thus we would like to cover the second part in detail next. Based on the automatic differentiation (AD) mechanism [46], the derivatives of the functions u and v are derived efficiently and accurately by computer programs. In the following, the loss function of the PINN system (84) consists of four parts, which are constructed as follows

$$Loss = Loss_I + Loss_{II} + Loss_{III} + Loss_{IV}, \tag{86}$$

with

$$\begin{cases} Loss_I = \left(\sum_{j=1}^{N_u} |\hat{u}(x_q^j, t_q^j) - u^j|^2 \right) / N_u, \\ Loss_{II} = \left(\sum_{j=1}^{N_u} |\hat{v}(x_q^j, t_q^j) - v^j|^2 \right) / N_u, \\ Loss_{III} = \left(\sum_{m=1}^{N_f} |f_u(x_f^m, t_f^m)|^2 \right) / N_f, \\ Loss_{IV} = \left(\sum_{m=1}^{N_f} |f_v(x_f^m, t_f^m)|^2 \right) / N_f. \end{cases} \tag{87}$$

The loss function is optimized by L-BFGS optimization method [47] to derive an relatively accurate prediction solution. It is worth mentioning that the PINN we constructed has 10 hidden layers with 50 neurons each. In addition, both the input layer and the output layer contain two neurons. The whole procedure is operated through Python 3.7 and run via Tensorflow 1.15.

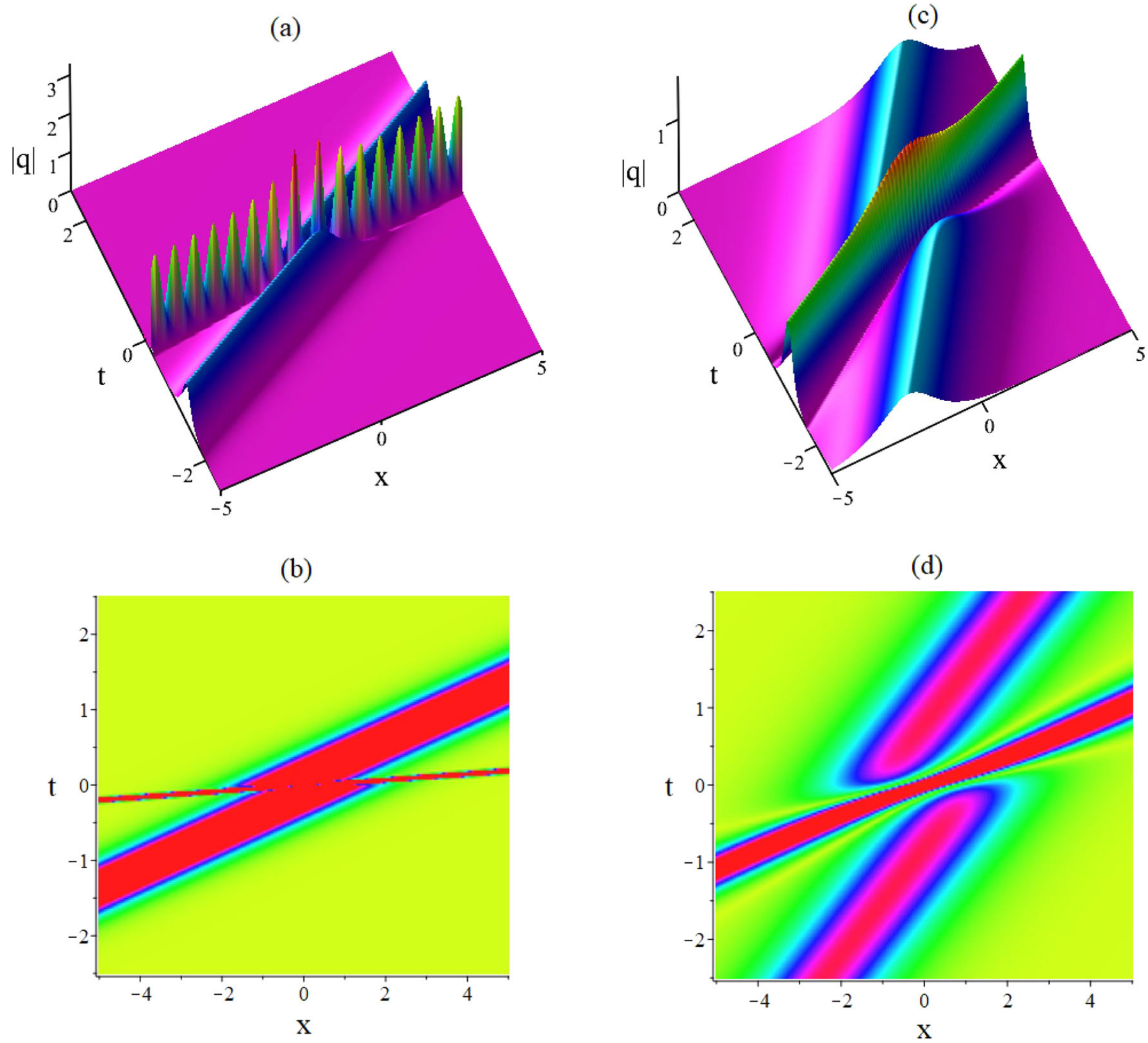

Fig. 4 Two-soliton given in (75) of the nonlocal SS equation (1). (a) and (b) with parameters: $(z_1, z_2) = (2.5i, i)$, $(\gamma_1, \gamma_2) = (1, 1)$. (c) and (d) with parameters: $(z_1, z_2) = (0.6i, i)$, $(\gamma_1, \gamma_2) = (1, 1)$

Then, we would like to derive data-driven solutions for the nonlocal SS equation (1) via simulations in the PINN algorithm, and then compare them with the exact solutions shown in the above section. Firstly, the line soliton solution shown in Fig. 3 is fitted by the PINN method, which is displayed in Fig. 6 with parameters $z_1 = 0.4i$ and $\gamma_1 = 2$. For this line soliton, the space and time ranges are taken as $[x_0, x_1] = [-3, 3]$ and $[t_0, t_1] = [-2, 2]$. To derive the discrete grid data, the spatial region is divided into 2000 points, and the temporal region is divided into 1000 points in MATLAB. Based on the discrete grid data in the spatio-temporal region, the original training data consists of random sampling points [48] which include $N_u = 1500$ points for the initial value and $N_f = 30000$ points for the inner points. In Fig. 6, the density images of exact and learned dynamics are given, where the darkness of the color is closely related to the height of the line soliton. In order to more intuitively observe the fitting of the predicted solution to the exact solution, we also show the vertical section diagrams at different times.

Secondly, we learn the oblique elastic collision between two line solitons shown in Fig. 4 (c) with parameters $(z_1, z_2) = (0.6i,\ i)$ and $(\gamma_1, \gamma_2) = (1,\ 1)$. In this time, we choose $[x_0, x_1] = [-4, 4]$ and $[t_0, t_1] = [-0.1, 0.1]$. Similar to the above, we also

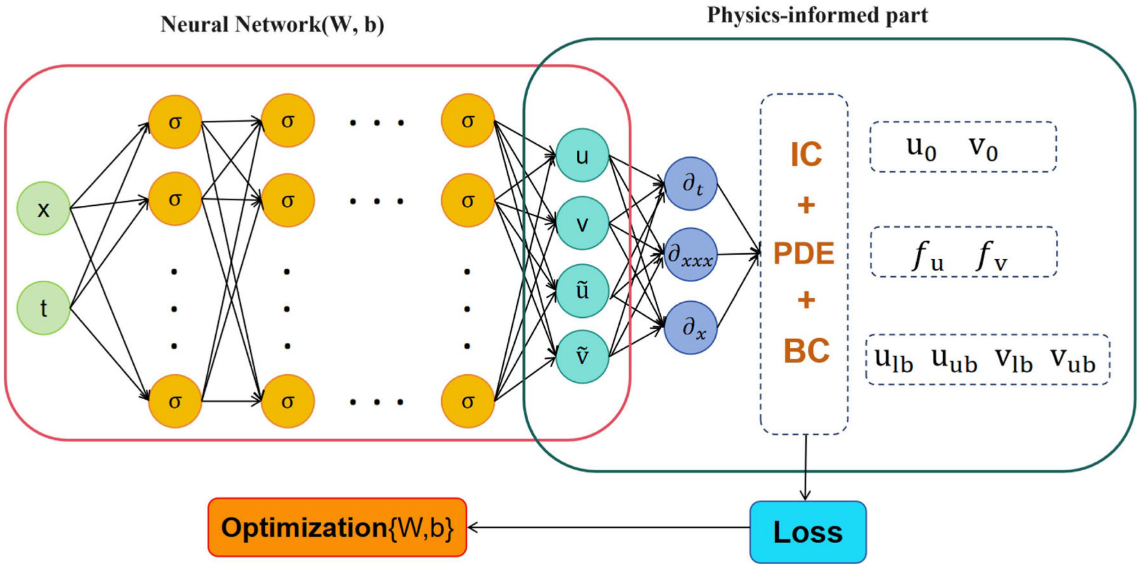

Fig. 5 Frame diagram of the PINN method with two main parts for the nonlocal SS equation. $\tilde{u}$ and $\tilde{v}$ represent $u(-x,-t)$ and $v(-x,-t)$, respectively

divide the discrete grid points to get the discrete grid data, and then derive the training data in the neural network. In Fig. 7, the density images and vertical section diagrams are shown the training results about the oblique elastic collision between two line solitons.

Thirdly, the breather-type solution shown in Fig. 1 (c) is learned via the PINN method, which is presented in Fig. 8 with parameters $z_1 = 0.5 + 0.5i$ and $(a_1, b_1, c_1, d_1) = (1 + 0.5i, -1 + i, 0.5 + i, -2 + 2i)$. For the breather-type solution of the nonlocal SS equation (1), we take the space and time ranges are $[x_0, x_1] = [-1.5, 3.5]$ and $[t_0, t_1] = [-0.01, 0.01]$. In Fig. 8, comparison results between the exact and predicted breather-type solutions are shown.

Through processing the training data, these data-driven solutions are learned by the PINN scheme. Figures 6-8 show these three sets of comparisons between the predicted data-driven solution and the exact solution from which it is clear that the error range is rather weak between the learned dynamics and exact dynamics. Thus, it is obvious that the PINN is an effective tool for describing solutions of the nonlocal SS equation (1) with initial and boundary conditions.

6 Conclusions

Firstly, this paper constructs nonlocal integrable SS hierarchies (20) by providing arbitrary order space-time spectral matrixes of zero curvature formula, which can deduce not only a novel nonlocal SS equation (1) but also a two-component nonlocal SS system. Furthermore, the Liouville integrability of these nonlocal hierarchies is illustrated by the bi-Hamiltonian structure. Secondly, through giving the Riemann-Hilbert problem and the symmetric constraints, we derive the precise expressions of N-soliton solutions, especially one-soliton and two-soliton, for the nonlocal SS equation (1) with space-time nonlocal terms. In order to intuitively display their dynamic characteristics, some figures are given to describe the one-soliton and two-soliton solutions. There are different dynamic with different parameters, such as a line soliton, breather-type solutions, and so on. Finally, we learn the data-driven solutions of the nonlocal SS equation (1) with the initial and boundary conditions by applying the PINN method, and then three comparison diagrams display the contrast between the exact dynamics and the predicted dynamics. The error range is rather weak between the learned data-driven solutions and exact calculated solutions, and the results show the PINN is an effective tool for describing solutions of the non-

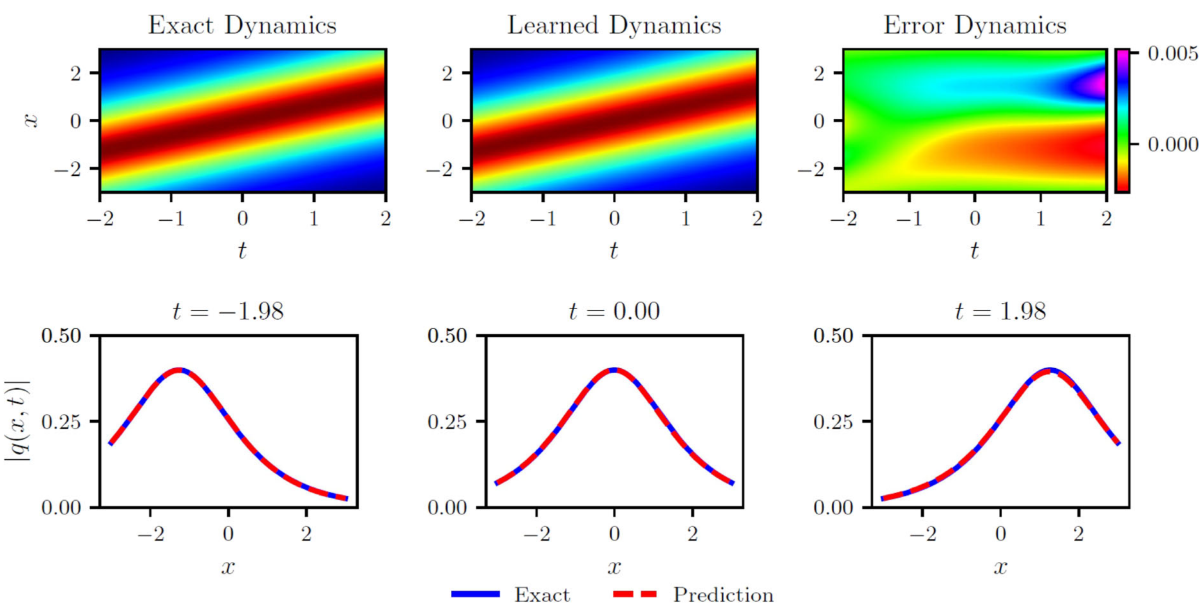

Fig. 6 Comparison diagram for the line soliton of the nonlocal SS equation(1): the error between the exact line soliton solution and the predicted data-driven solution

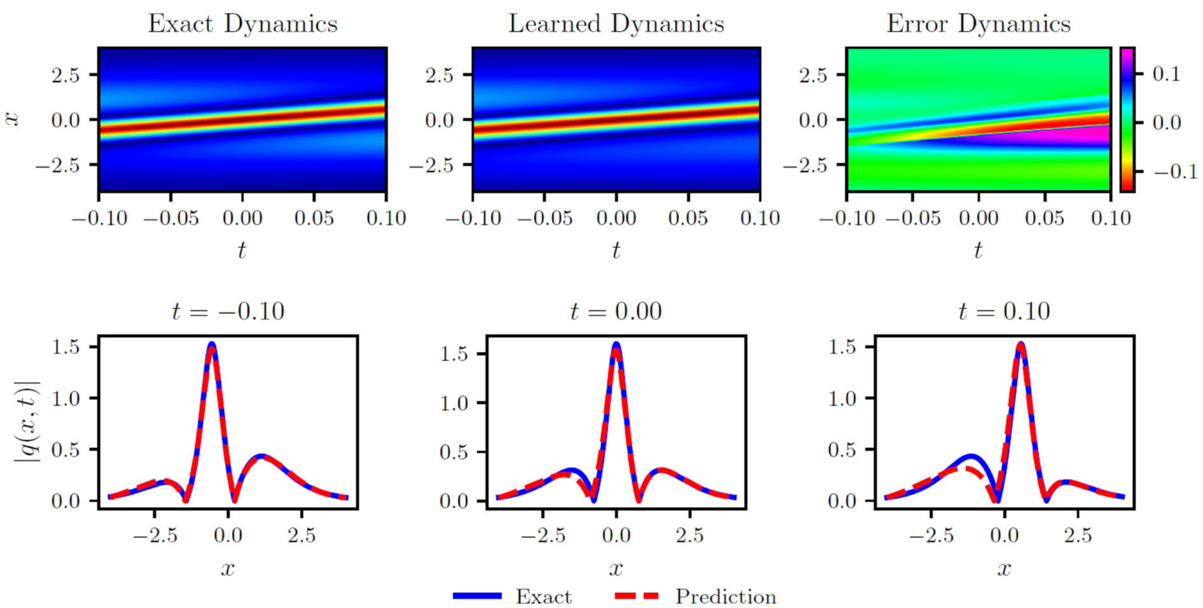

Fig. 7 Comparison diagram for the oblique elastic collision between two line solitons of the nonlocal SS equation (1): the error between the exact solution and the predicted data-driven solution

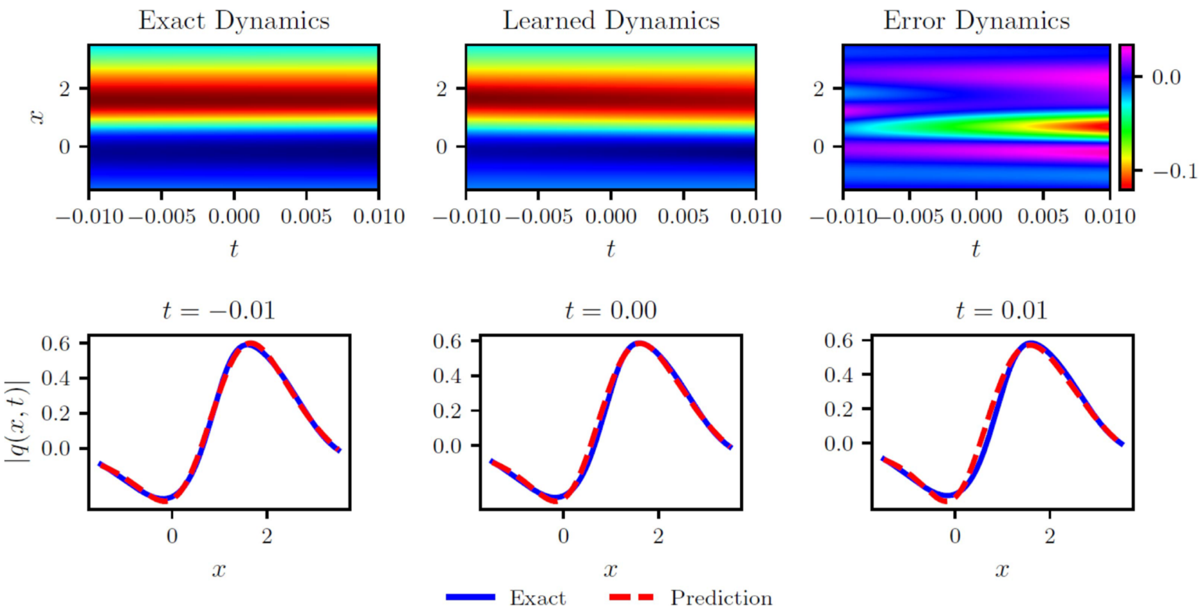

Fig. 8 Comparison diagram for the breather-type solution of the nonlocal SS equation (1): the error between the exact breather-type solution and the predicted data-driven solution

local SS equation (1) with the initial and boundary conditions. What's more, based on the nonlocal integrable SS hierarchies we construct, the Riemann-Hilbert problem and some soliton solutions for the nonlocal integrable hierarchies could be investigated. However, they go beyond the scope of this paper and will be studied in the future.

Acknowledgements The project is supported by National Natural Science Foundation of China (Nos. 12175069 and 12235007), Science and Technology Commission of Shanghai Municipality (Nos. 21JC1402500 and 22DZ2229014), and Natural Science Foundation of Shanghai (No.23ZR1418100).

Author contributions Both authors contributed to the work writing and review. Conceptualization, formal analysis and software were performed by Wen-Xin Zhang. Supervision, editing and project administration were performed by Yong Chen. The original draft of the manuscript was written by Wen-Xin Zhang and both authors commented on previous versions of the manuscript. Both authors read and approved the final manuscript.

Funding The work was supported by National Natural Science Foundation of China (Nos. 12175069 and 12235007), Science and Technology Commission of Shanghai Municipality (Nos. 21JC1402500 and 22DZ2229014), and Natural Science Foundation of Shanghai (No.23ZR1418100).

Data availibility All data analyzed during this work are included in this published article.

Declarations

Conflict of interest The authors declare that they have no known competing financial interests or personal relationships that could have appeared to influence the work reported in this paper.

References

1. Zakharov, V.E., Shabat, A.B.: Exact theory of two-dimensional self-focusing and one-dimensional self-modulation of waves in nonlinear media. Sov. Phys. JETP **34**, 62–69 (1972)
2. Chabchoub, A., Grimshaw, R.H.J.: The hydrodynamic nonlinear schrödinger equation: space and time. Fluids **23**, 1 (2016)
3. Ahmad, J., Akram, S., Noor, K., Nadeem, M., Bucur, A.B., Alsayaad, Y.: Soliton solutions of fractional extended nonlinear Schrödinger equation arising in plasma physics and nonlinear optical fiber. Sci. Rep. **13**, 10877 (2023)
4. Zakharov, V.E.: Collapse of langmuir waves. Sov. Phys. JETP **35**, 908–914 (1972)
5. Som, B.K., Gupta, M.R., Dasgupta, B.: Coupled nonlinear Schrödinger equation for Langmuir and dispersive ion acoustic waves. Phys. Lett. A **72**, 111–114 (1979)
6. Hosseini, K., Mirzazadeh, M., Gómez-Aguilar, J.F.: Soliton solutions of the sasa-Satsuma equation in the monomode

optical fibers including the beta-derivatives. Optik **224**, 165425 (2020)
7. Liu, L., Tian, B., Yuan, Y.Q., Du, Z.: Dark-bright solitons and semirational rogue waves for the coupled Sasa-Satsuma equations. Phys. Rev. E **97**, 052217 (2018)
8. Wu, C., Wei, B., Shi, C., Feng, B.F.: Multi-breather solutions to the Sasa-Satsuma equation. Proc. R. Soc. A. **478**, 20210711 (2022)
9. Wu, J.P., Geng, X.G.: Inverse scattering transform of the coupled Sasa-Satsuma equation by riemann-hilbert approach. Commun. Theor. Phys. **67**, 527–534 (2017)
10. Song, C.Q., Zhao, H.Q.: Dynamics of various waves in nonlinear Schrödinger equation with stimulated Raman scattering and quintic nonlinearity. Nonlinear Dyn. **99**, 2971–2985 (2020)
11. Wu, F., Huang, L.: Riemann-Hilbert approach and N-soliton solutions of the coupled generalized Sasa-Satsuma equation. Nonlinear Dyn. **110**, 3617–3627 (2022)
12. Wang, G., Wang, X.B., Long, H., Han, B.: Simple and high-order N-solitons of the nonlocal generalized Sasa-Satsuma equation via an improved Riemann-Hilbert method. Z. Angew. Math. Phys. **75**, 94 (2024)
13. Geng, X., Wu, J.: Riemann-hilbert approach and N-soliton solutions for a generalized Sasa-Satsuma equation. Wave Motion **60**, 62–72 (2016)
14. Yang, B., Chen, Y.: High-order soliton-matrices for Sasa Satsuma equation via local Riemann-Hilbert problem. Nonlinear Anal.-Real World Appl **45**, 918–941 (2019)
15. Liu, Y., Zhang, W.X., Ma, W.X.: Riemann-Hilbert problems and soliton solutions for a generalized coupled Sasa-Satsuma equation. Commun. Nonlinear Sci. Numer. Simul. **118**, 107052 (2023)
16. Ablowitz, M.J., Musslimani, Z.H.: Inverse scattering transform for the integrable nonlocal nonlinear Schrödinger equation. Nonlinearity **29**, 915–946 (2016)
17. Zhou, Z.X.: Darboux transformations and global explicit solutions for nonlocal davey-stewartson I equation. Stud. Appl. Math. **141**, 186–204 (2018)
18. Wang, X., He, J.: Darboux transformation and general soliton solutions for the reverse space-time nonlocal short pulse equation. Physica D **46**, 133639 (2023)
19. Wu, J.: A novel general nonlocal reverse-time nonlinear Schrödinger equation and its soliton solutions by Riemann-Hilbert method. Nonlinear Dyn. **111**, 16367–16376 (2023)
20. Zhang, Y., Dong, H.H.: N-soliton solutions to the multi-component nonlocal Gerdjikov-Ivanov equation via Riemann-Hilbert problem with zero boundary conditions. Appl. Math. Lett. **125**, 107770 (2022)
21. Song, C., Xiao, D., Zhu, Z.N.: Reverse space-time nonlocal Sasa-Satsuma equation and Its solutions. J. Phys. Soc. Jpn. **86**, 054001 (2017)
22. Wang, M., Chen, Y.: Novel solitons and higher-order solitons for the nonlocal generalized Sasa-Satsuma equation of reverse-space-time type. Nonlinear Dyn. **110**, 753–769 (2022)
23. Zhang, W.X., Liu, Y., Chen, X., Zeng, S.: Riemann-Hilbert problems and soliton solutions for the reverse space-time nonlocal Sasa-Satsuma equation. Nonlinear Dyn. **111**, 10473–10485 (2023)
24. Wang, G., Wang, X.B., Han, B.: Inverse scattering of nonlocal Sasa-Satsuma equations and their multisoliton solutions. Eur. Phys. J. Plus **137**, 404 (2022)
25. Ma, L.Y., Zhao, H.Q., Gu, H.: Integrability and gauge equivalence of the reverse space-time nonlocal Sasa-Satsuma equation. Nonlinear Dyn. **91**, 1909–1920 (2018)
26. Yang, B., Yang, J.: Transformations between nonlocal and local integrable equations. Stud. Appl. Math. **140**, 178–201 (2017)
27. Raissi, M., Perdikaris, P., Karniadakis, G.E.: Physics-informed neural networks: a deep learning framework for solving forward and inverse problems involving nonlinear partial differential equations. J. Comput. Phys. **378**, 686–707 (2019)
28. Raissi, M.: Deep hidden physics models: deep learning of nonlinear partial differential equations. J. Mach. Learn. Res. **19**, 932–955 (2018)
29. Sirignano, J., Spiliopoulos, K.: DGM: a deep learning algorithm for solving partial differential equations. J. Comput. Phys. **375**, 1339–1364 (2018)
30. Pu, J., Li, J., Chen, Y.: Solving localized wave solutions of the derivative nonlinear Schrödinger equation using an improved PINN method. Nonlinear Dyn. **105**, 1723–1739 (2021)
31. Zhou, Z., Yan, Z.: Deep learning neural networks for the third-order nonlinear Schrödinger equation: bright solitons, breathers, and rogue waves. Commun. Theor. Phys. **73**, 105006 (2021)
32. Wen, X.K., Wu, G.Z., Liu, W., Dai, C.Q.: Dynamics of diverse data-driven solitons for the three-component coupled nonlinear Schrödinger model by the MPS-PINN method. Nonlinear Dyn. **109**, 3041–3050 (2022)
33. Li, J., Li, B.: Mix-training physics-informed neural networks for the rogue waves of nonlinear Schrödinger equation. Chaos Solitons Fract. **164**, 112712 (2022)
34. Miao, Z.W., Chen, Y.: Physics-informed neural network method in high-dimensional integrable systems. Mod. Phys. Lett. B **36**, 2150531 (2022)
35. Lin, S., Chen, Y.: A two-stage physics-informed neural network method based on conserved quantities and applications in localized wave solutions. J. Comput. Phys. **457**, 111053 (2022)
36. Pu, J., Chen, Y.: Lax pairs informed neural networks solving integrable systems. J. Comput. Phys. **510**, 113090 (2024)
37. Song, J., Zhong, M., Karniadakis, G.E., Yan, Z.: Two-stage initial-value iterative physics-informed neural networks for simulating solitary waves of nonlinear wave equations. J. Comput. Phys. **505**, 112917 (2024)
38. Peng, W.Q., Chen, Y.: N-double poles solutions for nonlocal Hirota equation with nonzero boundary conditions using Riemann-Hilbert method and PINN algorithm. Physica D **435**, 133274 (2022)
39. Qiu, W.X., Si, Z.Z., Mou, D.S., Dai, C.Q., Li, J.T., Liu, W.: Data-driven vector degenerate and nondegenerate solitons of coupled nonlocal nonlinear Schrödinger equation via improved PINN algorithm. Nonlinear Dyn (2024). https://doi.org/10.1007/s11071-024-09648-y
40. Zhu, J., Chen, Y.: Data-driven solutions and parameter discovery of the nonlocal mKdV equation via deep learning method. Nonlinear Dyn. **111**, 8397–8417 (2023)

41. Zhang, Y., Liu, H., Wang, L., Sun, W.: The line rogue wave solutions of the nonlocal Davey-Stewartson I equation with PT symmetry based on the improved physics-informed neural network. Chaos Interdiscip. J. Nonlinear Sci. **33**, 013118 (2023)
42. Peng, W.Q., Chen, Y.: PT-symmetric PINN for integrable nonlocal equations: Forward and inverse problems. Chaos: Interdiscip. J. Nonlinear Sci. **34**, 043124 (2024)
43. Tu, G.Z.: On liouville integrability of zero-curvature equations and the Yang hierarchy. J. Phys. A: Math. Gen. **22**, 2375–2392 (1989)
44. Tu, G.Z.: The trace identity, a powerful tool for constructing the Hamiltonian structure of integrable systems. J. Math. Phys. **30**, 330–338 (1989)
45. Ma, W.X.: Variational identities and applications to hamiltonian structures of soliton equations. Nonlinear Anal. **71**, e1716–e1726 (2009)
46. Baydin, A.G., Pearlmutter, B.A., Radul, A.A., Siskind, J.M.: Automatic differentiation in machine learning: a survey. J. Mach. Learn. Res. **18**, 1–43 (2018)
47. Liu, D.C., Nocedal, J.: On the limited memory BFGS method for large scale optimization. Math. Program. **45**, 503–528 (1989)
48. Stein, M.: Large sample properties of simulations using latin hypercube sampling. Technometrics **29**, 143–151 (1987)